12th International Symposium on Turbulence and Shear Flow Phenomena (TSFP12)
Osaka, Japan (Online), July 19-22, 2022

EFFECT OF UPSTREAM BOUNDARY LAYER ON COHERENT STRUCTURES IN THE WAKE OF A BLUNT TRAILING EDGE PROFILED BODY

Ross Cruikshank & Philippe Lavoie
Institute for Aerospace Studies
University of Toronto
4925 Dufferin St., Toronto, Ontario, M3H 5T6, Canada
ross.cruikshank@mail.utoronto.ca & phil.lavoie@.utoronto.ca

ABSTRACT

The effect of the state of the upstream boundary layer and its thickness on the three-dimensional aspects of vortex shedding in the wake of a blunt trailing edge profiled body is investigated experimentally. Reynolds numbers based on body thickness, d, ranging from 2 800 to 38 000 and boundary layers with displacement thicknesses up to $0.38d$ are considered. Velocity field measurements of the near wake are made using hot-wire anemometry and particle image velocimetry (PIV). The PIV measurement plane is aligned with the trailing edge of the models, which allows the three-dimensional vortex shedding structures to be visualized. We assess the level of three-dimensionality through the spanwise correlation of the streamwise velocity, which is shown to be sensitive to both boundary layer transition and the thickness of the boundary layers. In all cases, the main three-dimensional features are oblique shedding and vortex dislocations. We find that, as the boundary layer transitions, the spanwise correlation drops and we link this to increased fluctuating vortex shedding phase drift along the span due to greater unsteadiness in the near wake velocity field. For the turbulent boundary cases, the fluctuating phase drift does not change significantly with boundary layer thickness. In this range, the main mechanism affecting the spanwise correlation is the relative strength of the vortex shedding compared to the random turbulent fluctuations in the wake.

INTRODUCTION

Wakes of bluff bodies are of interest due to how regularly they appear in engineering applications such as vehicles and structures. Two-dimensional bluff bodies commonly exhibit vortex shedding above a critical Reynolds number, and this leads to large periodic velocity fluctuations and unsteady loading. The geometry of interest in the present study is a blunt trailing edge (BTE) profiled body, shown schematically in Figure 1. This type of body has fixed separation points at the trailing edges. A fixed separation point removes some of the dependence of the flow field on the Reynolds number, compared to the variations exhibited for curved afterbodies. Nevertheless, the wake of a BTE body is still sensitive to the Reynolds number. If the incoming flow is spanwise uniform, then at Reynolds numbers less than about 210, the vortex shedding will also be two-dimensional (Petrusma & Gai, 1996). However, for Reynolds numbers greater than 210, the vortex shedding develops three-dimensional features irrespective of the initial conditions.

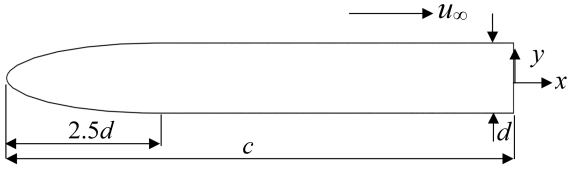

Figure 1: Schematic of the blunt trailing edge model and coordinate system

At relatively low Reynolds numbers, the three-dimensional features can be controlled through end-conditions. As the Reynolds number is increased, turbulence in the shear layers and wake begins to play a more important role in setting the three-dimensional structure, which can take several forms. Over long wavelengths, the von Kármán vortices may be shed at an angle, ψ, to the span of a bluff body, producing oblique vortex shedding. Vortex dislocations are associated with oblique shedding above a critical angle, wherein the vortex street assumes the pattern of a series of *cells* along the span. These *cells* may have different frequencies entirely, with phase discontinuities and a complex network of streamwise-oriented vortices connecting them (Williamson, 1992). Figure 2 shows a typical velocity field in the streamwise-spanwise plane of the wake to illustrate this. The coherent regions of high $u^\dagger = (u-\overline{u})/u_\infty$ roughly correspond to the locations of the von Kármán vortex cores. In this velocity field a dislocation exists at $z \approx -2d$, where the shedding exhibits a phase discontinuity. At $z \approx 2.5d$ the vortex shedding angle changes direction, but without a phase discontinuity.

The three-dimensional structure of a wake and the spanwise correlation are closely tied to the loading experienced by a bluff body. Firstly, the tilting of spanwise vorticity into streamwise vorticity reduces the strength of the shed vortices, and hence, the drag. Secondly, if the vortex shedding is out-of-phase across the span then the spanwise-varying induced forces leads to a reduced net load. Therefore, understanding the three-dimensional structure of wakes is essential for a proper interpretation of how the unsteady and overall loading varies for different bluff body geometries and flow conditions. Szepessy (1994) investigated the wake of a cylinder through the base pressure and found that the vortex shedding spanwise phase drift was the major contributor to the spanwise correlation at least up to the large subcritical Reynolds num-

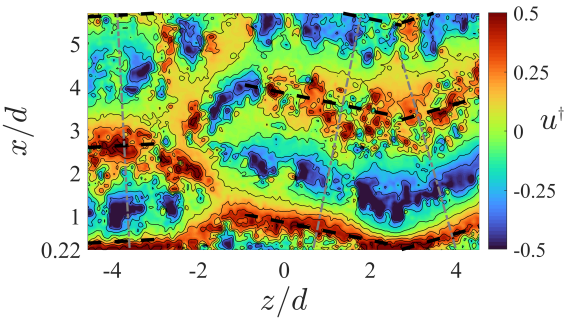

Figure 2: Sample velocity field in the $\{z,x\}$ plane aligned with the trailing edge at $\{Re_d = 20\,500, c = 12.5d\}$. The angle of the vortex shedding, ψ, is given as the dashed black lines. For $4.5d < z < -3d$, $\psi = 3°$, for $1d < z < 2.5d$, $\psi = -11.5°$, and for $2.5d < z < 4.5d$, $\psi = 16°$.

ber regime. Unlike for a cylinder, the chord length, c, of a BTE body can be varied independently of its thickness, d. Therefore, boundary layer thickness is decoupled from the Reynolds number based on body thickness, Re_d. Rai (2018) examined how the variability in the shedding frequency and strength for a bluff body were linked to streamwise vortices in the boundary layer. Vortex shedding unsteadiness is associated with three-dimensionality because the shedding frequency/strength must vary along the span for there to be a spanwise phase drift. The aim of this study is to gain a deeper understanding of how the two- and three-dimensional coherent structures in the wake change with both Re_d and boundary layer thickness. In order to better isolate the effect of Re_d and boundary layer thickness, both changes in c and u_∞ are considered. Furthermore, cases are considered where the boundary layer is either laminar or turbulent at separation.

METHODOLOGY

Experimental measurements were taken in a low freestream turbulence intensity ($< 0.1\%$) closed-circuit wind tunnel with an octagonal cross-section nominally 1.2 m by 0.8 m. Two BTE profiled models of identical thickness ($d = 25.4$ mm) and elliptical leading edge radius ($2.5d$) were used for the experiments. The first model has a length $c = 12.5d$ and a span of $26.8d$. Datasets at 5 different u_∞ were gathered, resulting in Re_d ranging from 2 800 to 20 500. The second model has a span of $30.3d$ and consists of six independent sections, allowing the overall length to be adjusted between $31d$ and $151d$. Three flow speeds were tested for the variable-length model, producing Re_d = 11 000, 22 000 and 38 000. To promote spanwise uniform and early transition to turbulence, the boundary layer is tripped on both sides of the leading edge sections, approximately $2.5d$ downstream of the leading edge. For the $c = 12.5d$ model, the trip is a strip of zig-zag tape of 9 mm width and 0.5 mm height and for the variable-length model, the trip is a roughness element 25 mm wide and 2 mm high. Both models are bounded by end-plates which extend upstream and downstream of the models.

Measurements of the flow for both models were made using single hot-wire anemometry, and two-component particle image velocimetry (PIV) in a $\{z,x\}$ plane aligned with the trailing edge at $y = 0.5d$, where the coordinate system is defined in Figure 1. A Dantec Type 55H probe and a Dantec 56C constant temperature anemometer were used for the hot-wire measurements. The hot-wires were made in-house on Dantec probes with 5 μm thick tungsten wire and sensing lengths of about 1.2 mm. Hot-wire measurements were made of the boundary layer velocity profiles at $0.5d$ upstream of the trailing edge, and at various locations in the near wake by positioning the wires with a three-axis traverse system. In the case of the $c = 12.5d$ model, each data point was sampled at 25 kHz with a 10.5 kHz low pass filter for 120 s. With the variable-length model, the sampling time and frequency were 120 s and 5 kHz with a 2 kHz low pass filter, respectively.

For the PIV measurements, the laser sheet was formed from a dual-pulse Nd-YAG laser and a series of lenses to direct the beam. A Lavision Imager sCMOS camera took the images. For all of the cases with the $c = 12.5d$ model, 3000 snapshots were taken, whereas 1000 snapshots were taken for the variable-length model cases. The $c = 12.5d$ cases had a field of view of $-4.5d < z < 4.5d$ and $0.22d < x < 5.7d$ with a vector spacing $0.043d$ and the vector fields with the variable-length model cases covered $-5.5d < z < 2.2d$ and $0.22d < x < 4.9d$, for a vector spacing $0.037d$. Lavision Davis 8.3.x software was used to process all the images, using window sizes of 16x16 pixels and 50% overlap.

RESULTS AND DISCUSSION

The boundary layer profiles for all the variable-length model cases indicate that the boundary layer is turbulent upstream of the trailing edge. The large scale two-dimensional properties of the vortex shedding are assessed through the velocity spectra in the wake. For the variable-length model, the velocity is measured by a hot-wire at $\{x,y\} = \{1.5d, 0.8d\}$ and all the spectra exhibit a prominent vortex shedding peak. Using the Strouhal number, $St = fd/u_\infty$, the spectral peak frequency, $\widehat{St}$, is found to range from $\approx 0.16 - 0.2$. Figure 3 shows that $\widehat{St}$ decreases with increasing δ^*/d, regardless of whether it is controlled through u_∞ or c/d. Similar observations for a BTE body were made by Rowe *et al.* (2000), except that they controlled the boundary layer only by using different surface roughness trips and did not isolate the effect of c/d. Boundary layer thickness effects the shedding period because it is related to the time it takes for a forming vortex to be cut off from its shear layer. According to the model of Gerrard (1966), the more diffuse the vorticity is, the longer it takes for the vorticity from a shear layer to be sufficiently drawn across the wake centerline and cut off the supply of vorticity to the opposite forming vortex. Additionally, more diffuse boundary layers/shear layers lead to weaker vortex shedding because the formed von Kármán vortices are less concentrated, irrespective of whether the boundary layer thickness is controlled through u_∞ or c/d.

With the $c = 12.5d$ model, the boundary layer is laminar for the $Re_d < 10\,000$ cases despite the trip at the leading edge, and between $Re_d = 10\,000$ and $Re_d = 16\,000$ the boundary layer transitions before it reaches the trailing edge. The velocity spectra computed from hot-wire measurements at $\{x,y\} = \{4d, 0.5d\}$ show that $\widehat{St}$ increases with Re_d while the boundary layer is laminar, ranging from $\widehat{St} \approx 0.23$ at $Re = 2\,800$ to 0.27 at $Re = 10\,000$. When the boundary layer transitions there is a step increase in its thickness, so $\widehat{St}$ decreases to 0.22 for the $Re_d \geq 16\,000$ cases. The fact that $\widehat{St}$ is higher in the turbulent boundary layer cases for $c = 12.5d$ than for the variable-length model cases is consistent with the more concentrated separated shear layers when c/d is shorter. The changes in $\widehat{St}$ with Re_d underscore that the vorticity thickness from the separated shear layers plays an important role in the shedding

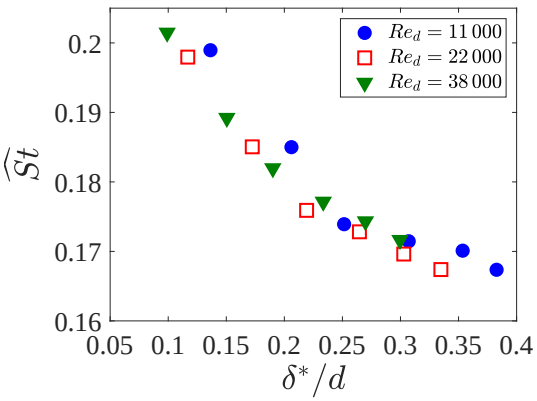

Figure 3: Dependence of $St(f_s)$ on δ^*/d for the variable-length model.

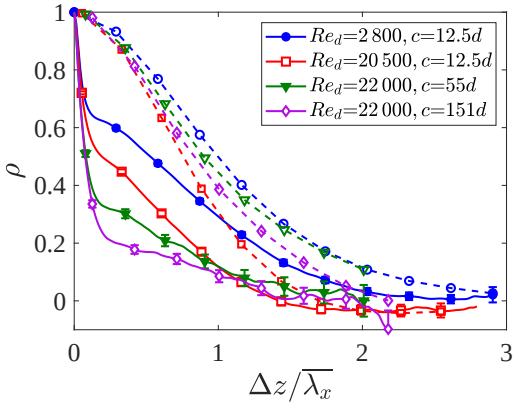

Figure 4: Spanwise cross-correlation as a function of spatial lag Δz for selected cases. ρ_u at $x = 3d$ in solid lines and ρ_ϕ in dashed lines.

frequency. Variations of the vorticity flux from the shear layers among different shedding cycles due to boundary layer disturbances can lead to unsteadiness in the shedding periods and amplitudes, in line with the experiments of Rai (2018). When the boundary layers transition, the levels of fluctuations in the shear layers increase. A key purpose of this study is to determine if these changes in the transitional boundary layer regime are connected to the levels of wake three-dimensionality.

The instant shown in Figure 2 illustrates that wake three-dimensionality and the overall correlation describes many features, notably the strength of the vortex shedding, the turbulence levels, secondary vortical structures, the phase drift/oblique shedding, and dislocation events. The overall spanwise coherence is assessed using the cross-correlation of u along z at constant x, defined as

$$\rho_u(x,\Delta z) = \frac{E\left[\Big(u(x,z)-\overline{u}(x,z)\Big)\Big(u(x,z+\Delta z)-\overline{u}(x,z+\Delta z)\Big)\right]}{\mathrm{var}\Big[u(x,z)-\overline{u}(x,z)\Big]} \tag{1}$$

Figure 4 plots $\rho_u(3d,\Delta z)$ for selected cases with the $c = 12.5d$ and variable-length model datasets. As measured in previous studies such as Bruun & Davies (1975) and Szepessy (1994), ρ_u declines with increasing Δz for all cases. For the $\{Re_d = 2\,800, c = 12.5d\}$ case, ρ_u is on average the highest at any given Δz. The drop in the correlation with increasing Re_d suggests that the wake is on average less organized. For the variable-length model cases, ρ_u is less sensitive to the different u_∞ and c/d investigated, presumably because the boundary layer is already turbulent in all these cases. The correlation length-scale, L_ρ, for the different cases was calculated by integrating the ρ_u curves to either the first zero-crossing or extrapolating them to zero.

The computed L_ρ for the various test cases are summarized in Figure 5. The results for the $c = 12.5d$ model show that the spanwise correlation drops rapidly when the boundary layer transitions to turbulence but stabilizes after transition for the $Re_d = 16\,000$ and $20\,500$ cases. This is consistent with the association of higher levels of turbulence in the near wake to increased wake unsteadiness and reduced vortex shedding organization. For the variable-length model cases, L_ρ generally declines with increasing δ^*/d, but does not collapse among the different Re_d with δ^*/d. While δ^*/d may be sufficient to characterize the large-scale two-dimensional vortex shedding properties such as $\widehat{St}$, this suggests that a full picture of the wake dynamics requires taking into account both Re_d and δ^*/d. We note that in general these values of L_ρ are lower than that measured for cylinder wakes at this Re_d range, which is nominally around $1\lambda_x$, where λ_x is the streamwise wavelength of the von Kármán vortex shedding (Bruun & Davies, 1975).

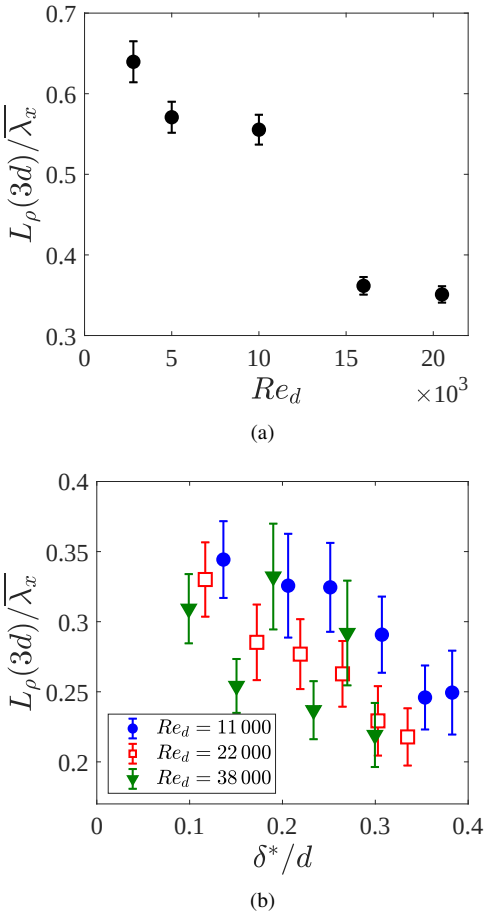

Figure 5: Variation of L_ρ, calculated at $x = 3d$ among the test cases with (a) the $c = 12.5d$ model with Re_d, and (b) the variable-length model with δ^*/d.

A limitation of this correlation analysis is that it does not take into account the various factors affecting the correlation, and is not reflective of the instantaneous variations in the correlation that may occur in time-varying flows like in the present case. The instantaneous snapshots vary considerably in the level of spanwise correlation they exhibit, with it not uncommon for some snapshots to have a correlation above 0.8 for all Δz. In other snapshots, the correlation drops to 0 with a distance of only $0.5\lambda_x$. This wide variation in spanwise correlation at different instants in time is consistent with the occurrence of unsteady three-dimensional features. Based on a close examination of the velocity fields in the $\{z,x\}$ plane, we find that the vortex shedding exhibits the same general types of large-scale three-dimensional structures (i.e., dislocations and oblique shedding) in all the investigated cases. Therefore, in Figure 5(a) and (b), the decrease in L_ρ with increasing Re_d and boundary layer thickness, respectively, may be reflective of 1) more dislocation events, 2) greater fluctuating phase drift across the span from oblique shedding (i.e., steeper and/or more frequent oblique shedding events), and/or 3) greater random small-scale fluctuations. These are important considerations in the generalization of these trends because they cannot be expected to vary in the same way with the mean shear layer velocity gradient and the fluctuations.

Because end-plates were used and oriented parallel to the freestream flow, instantaneous oblique shedding events are not driven by end-effects. Instead, phase drift in the investigated cases can be primarily attributed to turbulence in the shear layers and near wake causing spanwise variations in the vortex shedding. To isolate the correlation drop due to phase drift, we employ a novel algorithm to analyze the individual PIV snapshots to compute the shedding angle and phase across the span.

A central idea of our shedding angle identification algorithm is that by averaging along the direction of the von Kármán vortex lines, the small-scale fluctuations can be averaged out and what is left is representative of the large-scales directly associated with the vortex shedding. For some arbitrary angle, α, not necessarily aligned with the shedding angle, ψ, we can define transformed coordinates as

$$\begin{aligned} z_\alpha &= z\cos\alpha - x\sin\alpha \\ x_\alpha &= z\sin\alpha + x\cos\alpha \end{aligned} \tag{2}$$

For all $\alpha \neq 0^\circ$, averaging the velocity along z_α at constant x_α implies that the average is taken over varying x. Because the amplitude of the velocity fluctuations changes in the near wake with x, we take that into account by introducing $u^\ddagger$ to normalize u by the local rms velocity fluctuations: $u^\ddagger = (u-\overline{u})/u'$. Using the notation of $\langle\cdot\rangle$ to denote a spatial average, and the subscript to denote the direction angle of the spatial average, the average of $u^\ddagger$ along the z_α direction in a given region is expressed as $\langle u^\ddagger\rangle_\alpha$. The power associated with the long wavelength variations in $\langle u^\ddagger\rangle_\alpha$ along the x_α direction for a given region of a snapshot is represented symbolically as $\sigma(\alpha)$. It is calculated by integrating low frequency range in the power spectral density:

$$\sigma(\alpha) = \int_0^{\frac{1}{0.5\overline{\lambda_x}}} \mathrm{PSD}\left[\langle u^\ddagger(x_\alpha)\rangle_\alpha\right] \mathrm{d}f_{x,\alpha} \tag{3}$$

where $f_{x,\alpha}$ denotes the spatial frequency along the x_α direction, and the integral is calculated from $f_{x,\alpha}=0$ to $1/(0.5\overline{\lambda_x})$ to cover the long wavelength range that is associated with vortex shedding.

For α that are not very well aligned with the vortex shedding direction, the velocity spatial averages calculated from $\langle u^\ddagger(x_\alpha)\rangle_\alpha$ tend towards zero because $u^\ddagger$ is poorly correlated along lines of z_α. This produces low $\sigma(\alpha)$. When α is well-aligned with the vortex shedding direction, $u^\ddagger$ is strongly correlated along z_α. For example, in Figure 2 from $-1d < z < 2.5d$, the velocity field is well-correlated along the $\alpha = -11.5^\circ$ direction. In that case averaging $u^\ddagger$ along $z_\alpha = -11.5^\circ$ preserves the fluctuations associated with the vortex shedding and filters out the small-scale fluctuations; hence, $\sigma(-11.5^\circ)$ is the maximum. The best-fit shedding angle, ψ, for a given spanwise region is defined as the α with the maximum $\sigma(\alpha)$,

$$\psi = \mathrm{argmax}\left[\sigma(\alpha)\right] \tag{4}$$

This algorithm is what was used to determine the von Kármán vortex lines which are drawn in Figures 2. Additionally, a different algorithm is used to identify the locations of dislocations in the measured velocity fields and is able to stitch the shedding angle variations together along the span to maintain phase continuity of the vortex shedding everywhere that it is not broken by a dislocation. The details of this aspect of the analysis are not discussed in this paper. From the computed spanwise variations of the shedding angles, ψ, the spanwise phase drift, $\Delta\phi_z$, can be calculated in all the snapshots. These quantities are directly related to each other from geometry through λ_x for a given spanwise separation Δz as

$$\Delta\phi_z = 2\pi\frac{\Delta z\tan\psi}{\lambda_x} \tag{5}$$

With this approach we can obtain statistical distributions of $\Delta\phi_z$ as a function of Δz by using the information from all the records of the ψ variations in the measured velocity fields. We exclude phases differences across dislocations because there is no valid interpretation of ψ across a phase discontinuity in this context. The distributions of $\Delta\phi_z$ can be more efficiently summarized across all Δz by plotting their standard deviation to obtain a measure of the fluctuating phase drift. This is plotted for selected cases with the $c = 12.5d$ model and the variable-length model in Figure 6. Physically, the fluctuating phase drift is related to the probability of measuring a given shedding phase difference at a certain separation. As Δz increases, the fluctuating phase drift increases because there is more opportunity for the phase to drift in between two points with greater separation. Similar findings in the wake of a cylinder at $Re_d = 43\,000$ were reported by Szepessy (1994).

The fluctuating phase drift increases with Re_d as the boundary layer transitions to turbulence. This suggests that the increased velocity fluctuations in the shear layers as Re_d increases are associated with greater wake three-dimensionality, consistent with the decline of L_ρ when the boundary layer transitions. In contrast, for the variable-length model datasets, the fluctuating phase drift is not very sensitive to variations in Re_d or δ^*/d presumably because the boundary layer is turbulent in all those cases. This indicates that changes in boundary layer thickness after the boundary layer has transitioned only have a limited effect on the large-scale coherent three-dimensional properties of the vortex shedding for the BTE body. This suggests that the spanwise disturbances to the vortex shedding frequency and strength do not change nearly as much with Re_d

and δ^*/d in the range of investigation, as compared to the changes that happen when the boundary layer transitions.

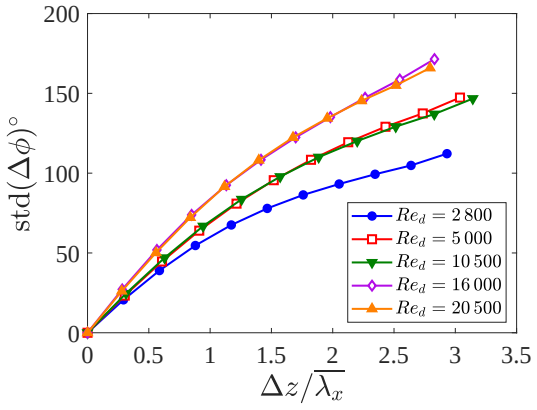

(a)

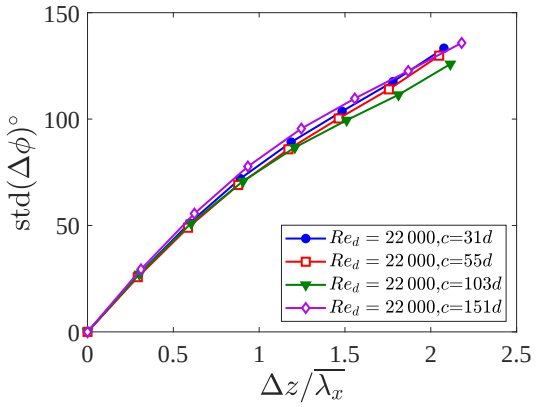

(b)

Figure 6: Fluctuating spanwise phase drift as a function of Δz. (a) For the $c = 12.5d$ cases, (b) Selected cases for the variable-length model.

Based on the work of Szepessy (1994), we can interpret the fluctuating phase drift in terms of a *phase*-based correlation coefficient. To make this interpretation, we represent the velocity at two spanwise separated positions as sine waves with the same frequency but phase shifted: $a = \cos\omega t$, and $b = \cos\omega t + \Delta\phi_z$. If we assume that $\Delta\phi_z$ varies in the snapshots independently of the shedding frequency, the phase-based correlation can be shown to be

$$\rho_\phi = \frac{1}{n}\sum_{i=1}^{n}\cos(\Delta\phi_{z,i}) \tag{6}$$

which is only a function of $\Delta\phi_z$. This is consistent with the general mathematical result that the correlation of two out of phase sine waves is simply $\cos(\Delta\phi_z)$. The value of interpreting the vortex shedding phase drift in this way is that it allows us to isolate its effect on the actual spanwise correlation measured from the velocity field. It removes the effect of turbulent fluctuations because the phase drift is a large-scale quantity that depends only on the vortex shedding, whereas the measured correlation from the velocity field is a superposition of all the possible three-dimensional effects.

Figure 4 plots ρ_ϕ for selected cases in dashed lines alongside the unconditional ρ_u with solid lines so that the relative values can be compared. The highest value of ρ_ϕ among the cases investigated is found for the $\{Re_d = 2\,800, c = 12.5d\}$ case, in agreement with the fluctuating phase drift curves of Figure 6. However, clearly the spanwise phase drift does not fully account for the drop in the spanwise correlation of the velocity with increasing Δz. A significant reason for the decline in ρ_u with Δz is related to the random turbulent fluctuations in the wake, which can obscure the vortex shedding signal. Changes in the random turbulent fluctuations among the different cases may be a driving factor for why ρ_u declines as the boundary layer thickness is increased for the turbulent boundary layer cases.

To investigate this possibility, we can compute the component of the spanwise correlation that removes the $\Delta\phi_z$ dependence. If as in Equation (6) we model $u(x,z)$ as being simply modulated along the span by the periodic von Kármán vortex shedding, then the effect of phase drift between two points can be accounted for in the typical correlation equation with an added $\cos(\Delta\phi_z)$ phase term:

$$\rho_{u|\Delta\phi_z}(x,\Delta z) = \frac{E\left[\Big(u(x,z)-\overline{u}(x,z)\Big)\Big(u(x,z+\Delta z)-\overline{u}(x,z+\Delta z)\Big)\cos(\Delta\phi_z)\right]}{\mathrm{std}\Big[u(x,z)-\overline{u}(x,z)\Big]\,\mathrm{std}\left[\Big(u(x,z)-\overline{u}(x,z)\Big)\cos(\Delta\phi_z)\right]} \tag{7}$$

We refer to $\rho_{u|\Delta\phi_z}$ as the spanwise correlation conditional on the phase drift. If there is any phase correlation between two points, $\rho_{u|\Delta\phi_z}$ must be higher than ρ_u. In the event that velocity differences between spanwise separated points are entirely a function of $\Delta\phi_z$, this would be reflected by a value of 1 for $\rho_{u|\Delta\phi_z}$. Conversely, if the vortex shedding phase difference between two points did not convey useful information (i.e., if there was no vortex shedding), $\rho_{u|\Delta\phi_z}$ would collapse onto ρ_u.

The variation of $\rho_{u|\Delta\phi_z}$ with Δz for selected variable-length model datasets is provided in Figure 7. It can be seen that $\rho_{u|\Delta\phi_z}$ declines sharply at small Δz, similar to ρ_u, but asymptotes to constant values at high Δz in every case. The reason for this is that at large separations, the random fluctuations in the wake tend to drive spanwise correlations to zero. The asymptotes of $\rho_{u|\Delta\phi_z}$ are non-zero in the present cases because even at large Δz, the wake flow is correlated via the vortex shedding. In other words, the von Kármán vortex street gives large-scale structure to the wake at large distances. The non-zero asymptotic values imply that if it were possible to enforce a parallel shedding condition in the turbulent boundary layer regime then there would still be a form of correlation even at large separations.

We can interpret the magnitude of the asymptotes for each case as being representative of the relative strength of the vortex shedding signal to the random fluctuations. This correspondence is illustrated by comparing Figure 7 to Figure 8. Figure 8 expresses the *relative* power of the vortex shedding signal to the total velocity fluctuations measured by the hot-wire at $\{x = 1.5d, y = 0.8d\}$. The power is calculated by integrating the shedding spectral peaks around the 3 dB (half power) bandwidth. Figure 8 shows that the relative power of the vortex shedding power decreases with δ^*/d, so it is increasingly dominated by random fluctuations as the boundary layer thickness near the trailing edge grows. This explains why ρ_u declines with increasing δ^*/d for the variable-length model cases even though the underlying large-scale three-dimensional structure and overall phase drift does not significant change in this range.

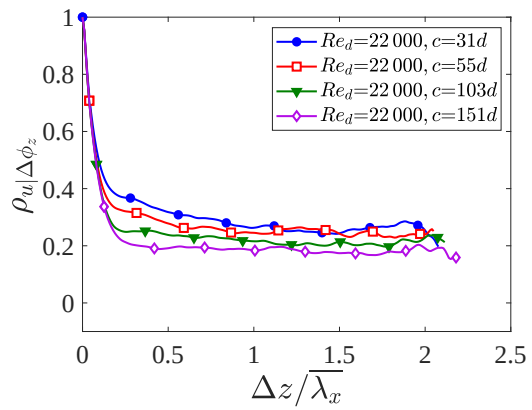

Figure 7: Spanwise correlation conditional on the phase drift, $\rho_{u|\Delta\phi_z}$, as a function of spatial lag Δz for selected cases with the variable-length model.

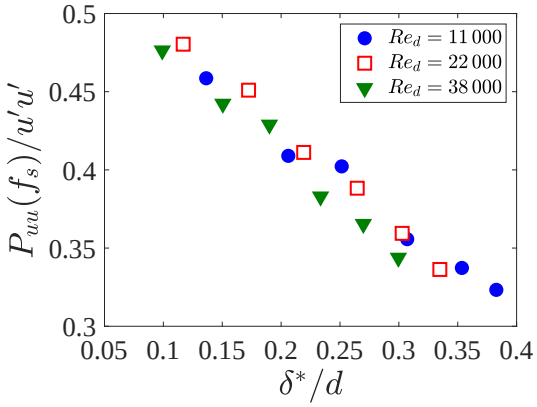

Figure 8: Relative vortex shedding power to the overall fluctuations as measured at $\{x,y\} = \{1.5d, 0.8d\}$ for the variable-length model.

CONCLUSION

The large-scale two-dimensional and three-dimensional properties of the vortex shedding in the near wake of a blunt trailing edge profiled body have been experimentally examined. A central question in this study was the effect of boundary layer transition and its thickness on the wake coherent structures, which we characterize through spanwise correlations. To this end, Re_d was varied from 2 800 to 38 000 and the boundary layer thickness was controlled via u_∞ and model length. In all cases the vortex shedding was found to exhibit significant spanwise phase drift and dislocations. Because parallel end-plates were used, this phase drift is due to intrinsic spanwise variations that develop as the flow convects over the bodies, driven by turbulence in the shear layers and near wake. When Re_d was increased while the boundary layer was laminar at separation, the correlation length, $L_\rho(3d)$, dropped from approximately $0.65\overline{\lambda_x}$ to $0.55\overline{\lambda_x}$. The transition to turbulence in the boundary layer caused a more considerable drop in $L_\rho(3d)$ from about $0.55\overline{\lambda_x}$ to $0.35\overline{\lambda_x}$, which is indicative of the high sensitivity of wake three-dimensionality to the state of the upstream boundary layer.

To examine the connection between the spanwise correlation and the shedding phase drift, an algorithm was developed to compute the instantaneous vortex shedding angles/phase drift along the span from the velocity field measurements. The phase drift fluctuations were found to increase significantly with increasing separation between points in all investigated cases, which is consistent with the measured decline in the velocity correlation with increasing separation. This connection between the phase drift and correlation was further explored by computing a *phase*-based correlation which is dependent only on the spanwise phase drift. The fluctuating phase drift was found to increase with Re_d in the boundary layer transitional regime, which is consistent with the link between greater unsteadiness in the shear layers and weaker wake spanwise correlation. In contrast, varying the boundary layer thickness in the turbulent boundary layer regime did not have an appreciable effect on the fluctuating phase drift.

The phase-based correlation was not entirely predictive of the velocity correlation, underscoring that another important factor that affects the spanwise correlation of the velocity is the turbulent fluctuations in the wake. These fluctuations can be envisioned as essentially random disturbances to the coherent vortex shedding signals which tend to decorrelate the velocity field with increasing separation. When the vortex shedding is strong relative to the turbulent fluctuations, we found that the spanwise correlations are dominated by the large-scale vortex shedding component, but as the vortex shedding got weaker, the random fluctuations played a larger role. Increasing δ^*/d weakens the vortex shedding relative to the other velocity fluctuations in the wake, and so the spanwise correlation in the velocity field is progressively more affected by random fluctuations. These trends may have implications on possible ways to extrapolate measured spanwise velocity correlations to higher δ^*/d or Re_d in the turbulent boundary layer regime.

REFERENCES

Bruun, H.H. & Davies, P.O.A.L. 1975 An experimental investigation of the unsteady pressure forces on a circular cylinder in a turbulent cross flow. *J. Sound Vib.* **40** (4), 535–559.

Gerrard, J. 1966 The mechanics of the formation region of vortices behind bluff bodies. *J. Fluid Mech.* **25** (2), 401–413.

Petrusma, M. & Gai, S. 1996 Bluff body wakes with free, fixed, and discontinuous separation at low reynolds numbers and low aspect ratio. *Exp. Fluids* **20**, 189–198.

Rai, M. 2018 Vortex shedding characteristics of the wake of a thin flat plate with a circular trailing edge. *Int. J. Heat and Fluids Flow* **72**, 20–36.

Rowe, A., Fry, A. & Motallebi, F. 2000 Influence of boundary-layer thickness on base pressure and vortex shedding frequency. *AIAA J.* **39** (4), 754–756.

Szepessy, S. 1994 On the spanwise correlation of vortex shedding from a circular cylinder at high subcritical reynolds number. *Phys. Fluids* **6**, 2406–2416.

Williamson, C.H.K. 1992 The natural and forced formation of spot-like vortex dislocations in the transition of a wake. *J. Fluid Mech.* **243**, 393–441.